Multi-Dimensional Modelling of Atmospheric Pressure Discharge in Helium-Air Gas Mixture

M. M. Iqbal[1], M. M. Turner[1]

[1]*National Centre for Plasma Science and Technology, Dublin City University, Glasnevin, Dublin 9, Dublin, Ireland.*

Introduction:

In this numerical study, an effective understanding of atmospheric pressure discharge (APD) is developed by an analysis of the physical properties of discharge species under different conditions in He-air operating gas. The multi-dimensional coupled system of fluid model equations are numerically solved for the weakly ionized discharge plasma in the presence of neutrals, metastables, excimers, ionic species and clusters, such as He^+, He_2^+, N_2^+, O_2^+, O^+, N^+, NO^+, O_4^+, N_4^+, H_2O^+, H_3O^+, $H_2O.H_3O^+$, e^-, O^-, O_2^-, O_3^-, O_4^-, CO_3^-, CO_4^-, He(2^3S and 2^1S), $He_2(a^3\sum_u^+)$, $O^*(^1D)$ and $O^*_2(^1\Delta_g)$ in two and three-dimensional space. To illustrate the complexity of APD in He-air gas, the reaction rates of 80 chemical reactions, such as direct excitation and ionization of gas mixture atoms, Penning ionization of air gas impurities, charge transfer, attachment of electrons and dissociative recombination processes from the various sources are considered to explore the characteristic features of discharge kinetics with multi-dimensional numerical simulations [1 - 3].

Results and Discussion:

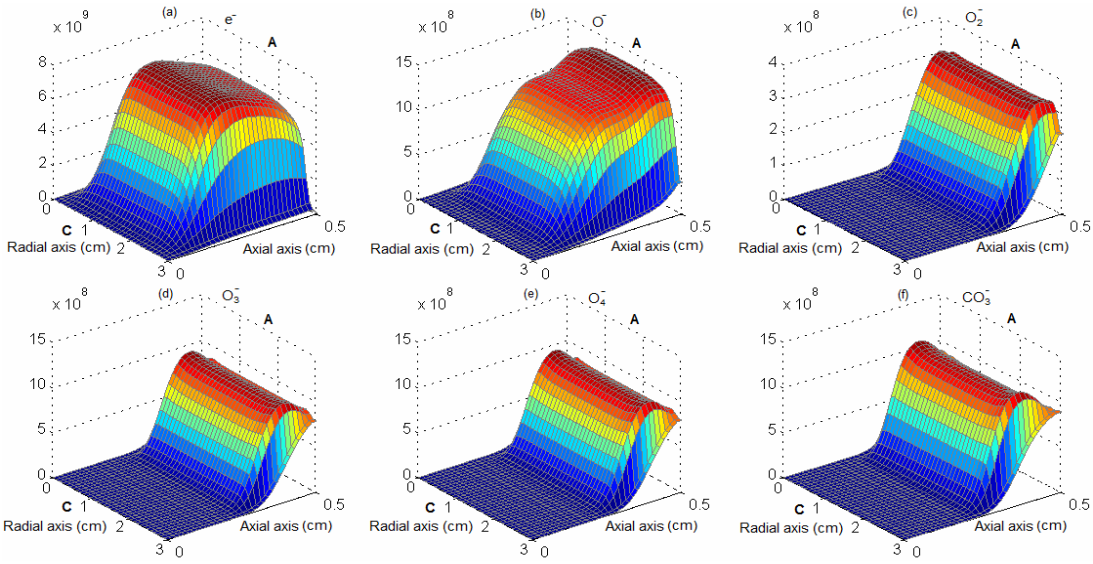

Figure 1 (a - f): Two-dimensional profiles of electrons, O^-, O_2^-, O_3^-, O_4^- and CO_3^- at 30 kHz and 1.5 kV.

The distinct behaviour of atmospheric pressure discharge is substantially emerged during the progression of initialization, growth and decay phases of a half cycle but the prominent

interacting activities of discharge participating species are involved in the breakdown phase. The pattern of spatial distributions of electrons and negative ionic species density are described in the breakdown phase as shown in figure 1 (a - f), when their sharp peaks exist near the momentary cathode (C) and anode (A) barriers at the maximum conduction discharge current density. As the electrons acquire maximum density in the negative glow region during the development of uniform glow discharge plasma as displayed in figure 1 (a), the noticeable quantity of O^- ions is also present in the positive column and its maximum value exists near the momentary anode barrier as shown in figure 1 (b). In He-air APD, the O^- ions are produced due to the major contribution of electrons attachment with the atomic oxygen, while they sharply transform into negative molecular ions and dissociate through the multiple channels of recombination. The strong generation of electrons is balanced with the attachment processes, which provide the formation of these negative ions (O_2^-, O_3^-, O_4^-, CO_3^- and CO_4^-). It is apparent from the figure 1 (c - f) that the higher densities of negative ions (O_2^-, O_3^-, O_4^- and CO_3^-) are turned up in the form of sharp distorted profiles near the momentary anode barrier as compared to the electrons and O^- ions.

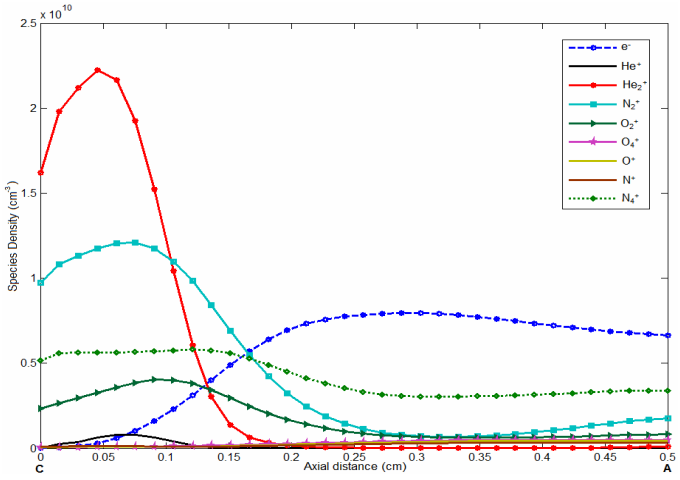

Figure 2: One-dimensional line mean densities of electrons and positive ions at 30 kHz and 1.5 kV in He-air gas.

The line averaged density of electrons and positive ions are elaborated by their spatial profiles during the formation of cathode fall layer in the glow discharge phase. It is evident from the spatial distribution of discharge species that the sharp peak corresponds to the molecular helium ions as compared to other ions in the cathode fall region. The higher densities of molecular nitrogen and oxygen impurity ions are observed near the cathode barrier (C) and become small in the positive column as exhibited in figure 2. The expressive amount of N_4^+ ions is evolved throughout the reactor gap, whereas the smaller densities of atomic and molecular ions (He^+, O^+, N^+ and O_4^+) are perceived in the positive column than other heavy ionic species. The above spatial profile enhance an overall view of electrons and major

positive ionic species in the atmospheric pressure discharge.

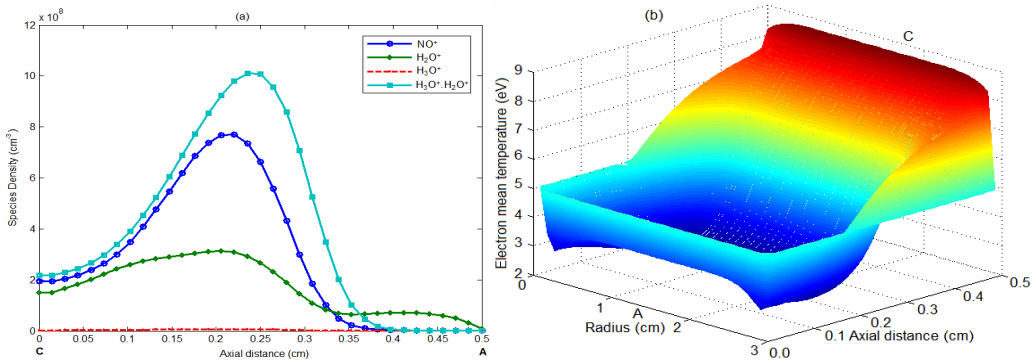

Figure 3 (a, b): One-dimensional line averaged density of ionic species and clusters, and two-dimensional structure of electron mean temperature for f = 30 kHz and V_{appl} = 1.5 kV in He-air gas.

The spatial investigation of one-dimensional structure of some positive ionic species and clusters exhibit that they are dominant in the central portion of reactor as shown in figure 3 (a) because of intense collisions at atmospheric pressure. This is confirmed with the maximum densities of NO^+, H_2O^+ ions and $H_3O.H_2O^+$ in this particular region and the cluster, $H_3O.H_2O^+$ is emerged as one of the distinguished species in the mentioned heavy ionic species. The different amounts of impurities (N_2, O_2 and CO_2) in He-air gas perform an important role to modify the discharge kinetics with Penning ionization process than the pure helium gas. Accordingly, the electrons in the discharge plasma absorb energy from the mean electric field, which is clearly distorted near the cathode barrier as illustrated in figure 3 (b). The electron density becomes very small in the cathode fall layer and the positive ions are responsible for the energy transformation in this region. The electron mean temperature is indicated with an abrupt falling trend in the cathode fall region, which reduces from the higher to lower values and slightly rises again near the anode barrier. The magnitude of electron mean temperature is varied from ~ 8.5 to 3.0 eV near the momentary cathodic barrier.

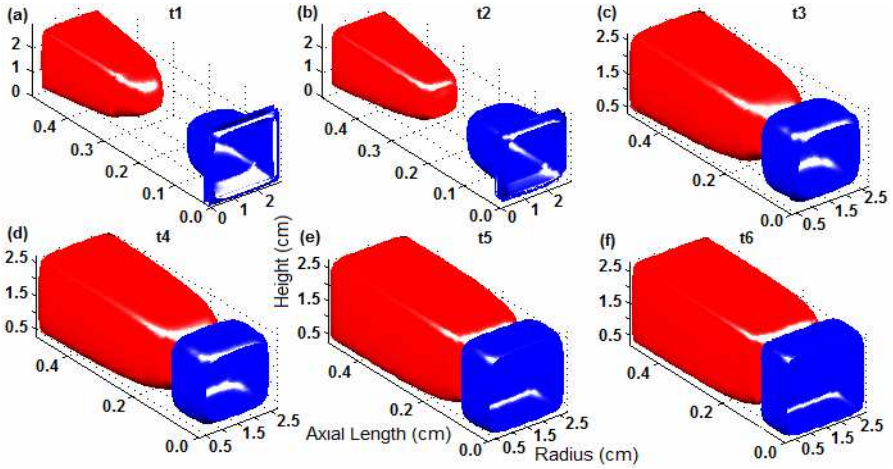

Figure 4 (a - f): Volumetric distributions of He_2^+ ions (blue) and e^-s (red) at 30 kHz and 1.5 kV in He-N_2 gas.

The evolution of homogeneous uniform volumetric distributions of electrons and He_2^+ ions densities are discussed from the time t1 to t6 in three-dimensional space for 30 kHz driving frequency as shown in figure 4 (a - f). Initially, the spatial structures of electrons and He_2^+ ions density are examined in the pre-breakdown phase as displayed in figure 4 (a - c) from t1 to t3 with an interval of ~ 1 μs. In the last structure of pre-breakdown as expressed in 4 (c), the electrons and He_2^+ ions densities acquire the numerical values of ~ 5.0×10^9 and 1.0×10^{10} cm^{-3}. The figure 4 (d) exhibits the species density in the start of breakdown phase at t4, while the electrons and ions proceed towards their respective anode and cathode barriers. The densities of electrons and He_2^+ ions are increased to further higher values in the start of breakdown pulse and reached to the magnitudes ~ 6.0×10^9 and 1.6×10^{10} cm^{-3}. The rapid movement of electrons represent that the ionization flit quickly travels towards the cathode barrier and the volumetric densities of electrons and He_2^+ ions rise to ~ 8.0×10^9 and 2.6×10^{10} cm^{-3} as illustrated in figure 4 (e). However, the three-dimensional profiles of electrons and He_2^+ ions density demonstrate that the electrons are occupied in the larger space due to their higher mobility and kinetic interaction with other species in the reactor gap and the He_2^+ ions are squeezed in the smaller space near the surface of cathode barrier. The volumetric structure of electrons and He_2^+ ions in figure 4 (f) corresponds to the homogeneous uniform distribution of atmospheric pressure discharge with the identification of four distinct regions in the gap, while the time span between t3 to t6 is approximately ~ 2 μs. The change in He_2^+ ions density is larger than electrons and it varies from ~ 4.0×10^9 and 3.0×10^{10} cm^{-3}, while the density of electrons alters from ~ 3.0×10^9 and 8×10^9 cm^{-3} during the time interval from t1 to t6. Consequently, the evolvement of pre-breakdown, breakdown and formation of cathode fall layer are recognized from the spatio-temporal distributions of electrons and He_2^+ ions densities. Thus the dynamic activities of electrons and He_2^+ ions can be sharply observed from the analysis of above six distributions, which develop a smooth and profound impression of initialization and breakdown phases of a half cycle [4] in three-dimensional space.

References

[1] K. R. Stalder, G. Nersisyan and W. G. Graham, J. Phys. D: Appl. Phys. 39, 3457-3460, 2006.

[2] M. H. Bortner and T. Baurer, Defense Nuclear Agency Reaction Rate Handbook, Second Edition, Section 24 Revision No. 7, March 1978, NTIS AD-763699, 1979.

[3] R. J. Vidmar, Plasma Cloaking: Air chemistry, Broadband Absorption, and Plasma generation, Air force office of scientific research, Final report, February 1990.

[4] M. M. Iqbal, M. M. Turner, Proceeding in 29th ICPIG, July 12-17, 2009, Cancún, México.